Received: 15 February 2022 | Revised: 1 July 2022 | Accepted: 5 July 2022

DOI: 10.1002/jev2.12246

RESEARCH ARTICLE

Metabolic labeling of cardiomyocyte-derived small extracellular-vesicle (sEV) miRNAs identifies miR-208a in cardiac regulation of lung gene expression

Chaoshan Han[1] | **Junjie Yang**[1] | **Eric Zhang**[1] | **Ying Jiang Data curation|Supporting**[1] | **Aijun Qiao Visualization|Supporting**[1] | **Yipeng Du Data curation|Supporting**[1] | **Qinkun Zhang Methodology|Supporting**[2] | **Junqing An Methodology|Supporting**[3] | **Jiacheng Sun Methodology|Supporting**[1] | **Meimei Wang Methodology|Supporting**[1] | **Thanh Nguyen Methodology|Supporting**[1] | **Hind Lal Methodology|Supporting**[2] | **Prasanna Krishnamurthy Methodology|Supporting**[1] | **Jianyi Zhang**[1] | **Gangjian Qin**[1]

[1]Department of Biomedical Engineering, School of Medicine and School of Engineering, University of Alabama at Birmingham, Birmingham, Alabama, USA

[2]Department of Medicine, Division of Cardiovascular Disease, School of Medicine, University of Alabama at Birmingham, Birmingham, Alabama, USA

[3]Center for Molecular and Translational Medicine, Georgia State University, Atlanta, Georgia, USA

Correspondence
Gangjian Qin, Molecular Cardiology Program, Department of Biomedical Engineering, School of Medicine & School of Engineering, University of Alabama at Birmingham, 1720 2nd Ave S, Volker Hall G094N, Birmingham, AL 35294, USA.
Email: gqin@uab.edu

Abstract

Toxoplasma gondii uracil phosphoribosyltransferase (UPRT) converts 4-thiouracil (4TUc) into 4-thiouridine (4TUd), which is incorporated into nascent RNAs and can be biotinylated, then labelled with streptavidin conjugates or isolated via streptavidin-affinity methods. Here, we generated mice that expressed *T. gondii* UPRT only in cardiomyocytes (^{CM}UPRT mice) and tested our hypothesis that CM-derived miRNAs (^{CM}miRs) are transferred into remote organs after myocardial infarction (MI) by small extracellular vesicles (sEV) that are released from the heart into the peripheral blood (^{PB}sEV). We found that 4TUd was incorporated with high specificity and sensitivity into RNAs isolated from the hearts and ^{PB}sEV of ^{CM}UPRT mice 6 h after 4TUc injection. In ^{PB}sEV, 4TUd was incorporated into CM-specific/enriched miRs including miR-208a, but not into miRs with other organ or tissue-type specificities. 4TUd-labelled miR208a was also present in lung tissues, especially lung endothelial cells (ECs), and CM-derived miR-208a (^{CM}miR-208a) levels peaked 12 h after experimentally induced MI in ^{PB}sEV and 24 h after MI in the lung. Notably, miR-208a is expressed from intron 29 of α myosin heavy chain (αMHC), but αMHC transcripts were nearly undetectable in the lung. When ^{PB}sEV from mice that underwent MI (MI-^{PB}sEV) or sham surgery (Sham-^{PB}sEV) were injected into intact mice, the expression of Tmbim6 and NLK, which are suppressed by miR-208a and cooperatively regulate inflammation via the NF-κB pathway, was lower in the lungs of MI-^{PB}sEV–treated animals than the lungs of animals treated with Sham-^{PB}sEV or saline. In MI mice, Tmbim6 and NLK were downregulated, whereas endothelial adhesion molecules and pro-inflammatory cells were upregulated in the lung; these changes were significantly attenuated when the mice were treated with miR-208a antagomirs prior to MI surgery. Thus, ^{CM}UPRT mice enables us to track ^{PB}sEV-mediated transport of ^{CM}miRs and identify an miR-208a-mediated mechanism by

which myocardial injury alters the expression of genes and inflammatory response in the lung.

KEYWORDS
endothelial cells, extracellular vesicles, lung, miR-208a, myocardial infarction, UPRT

1 | INTRODUCTION

Ischemic heart disease (IHD) is the leading cause of death worldwide (Virani et al., 2020), and although investigations of IHD have frequently focused on the progression from acute myocardial infarction (MI) to adverse remodelling and heart failure, the pathological mechanisms induced by the initial infarct event are not restricted to the cardiovascular system (Prabhu & Frangogiannis, 2016). For example, acute MI induces pulmonary edema and the proliferation of parenchymal cells, as well as pulmonary fibrosis and the thickening of inter-alveolar septa, which can contribute to the development of pulmonary hypertension and heart failure (Biddle et al., 1974; Guazzi et al., 2008; Hales & Kazemi, 1974; Hu et al., 2017; Jasmin et al., 2004; Mlczoch & Kaindl, 1980). Thus, a better understanding of how cardiomyocytes (CMs) regulate the activity of cells in other organs, such as the lung, may aid the development of effective therapies for improving outcomes in patients with IHD.

Extracellular vesicles (EV) are lipid-bilayer membranous particles released by all cell types (Deatherage & Cookson, 2012; O'Brien et al., 2020; Robinson et al., 2016). They carry bioactive molecules (proteins, RNAs, microRNAs [miRs], and metabolites) that modulate the activity of target cells (de Couto et al., 2017; Huang et al., 2021; Peinado et al., 2012; Valadi et al., 2007). In particular, EV that are produced by cardiac cells and released into the peripheral blood are key mediators of communication between the heart and other organs (Bei et al., 2017; Cheng et al., 2019; Gholamin et al., 2016) and can have an important role in cardiovascular disease (de Abreu et al., 2020; Gao et al., 2020; Garikipati et al., 2018; Kishore & Khan, 2017; Loyer et al., 2018; Oh et al., 2020; Sahoo & Losordo, 2014; Youn et al., 2019). Cardiac EV are taken up by cells in the thymus, lung, and kidney (Luo et al., 2020) and appear to promote cardiac fibrosis by transporting miR-208a, which is expressed primarily in CMs, to fibroblasts (Yang et al., 2018). Notably, we have shown that EV in the peripheral blood (^{PB}EV) of patients who have experienced an acute MI contain elevated levels of miR-208 and other CM miRs, and that ^{PB}EV collected from mice after MI potently mobilize bone marrow (BM) progenitor cells when administered to intact mice (Cheng et al., 2019). However, most studies of EV-mediated miR delivery have been conducted with exogenously administered EV, because techniques for distinguishing between the EV produced by CMs (^{CM}EV) and those from other organs or tissues within the same animal are lacking, so the roles of endogenously produced CM miRs in remote organs and tissues remain largely uncharacterized (Barile et al., 2017; O'Brien et al., 2020; Verweij et al., 2021).

EV are broadly divided into two major categories, exosomes and ectosomes (i.e., microvesicles); exosomes are formed in the multivesicular endosomes (MVEs; or multi-vesicular bodies, MVBs) as intraluminal vesicles (ILVs) and released into extracellular space upon fusion of MVBs with the cell membrane (Baietti et al., 2012; van Niel et al., 2018), whereas microvesicles are generated by direct outward budding of plasma membrane of the cell. Thus exosomes and microvesicles have same membrane orientation identical to that of the cell surface, but are different in size (exosomes at 30–150 nm vs. ectosomes at 50–2000 nm in diameter) (Raposo & Stoorvogel, 2013; Raposo et al., 1996) and cargo compositions (Yanez-Mo et al., 2015; Zaborowski et al., 2015). Small EV (sEV, $<$ 200 nm in diameter) are enriched for exosomes, whereas large EV (lEV, $>$ 200 nm in diameter) are enriched for microvesicles.

Unlike its orthologue in mammals, the uracil phosphoribosyltransferase (UPRT) of *Toxoplasma gondii* converts 4-thiouracil (4TUc) into 4-thiouridine (4TUd), which is incorporated into newly transcribed RNAs (Cleary et al., 2005; Gay et al., 2013; Gay et al., 2014; Herzog et al., 2017; Sharma et al., 2018; Tomorsky et al., 2017; Zeiner et al., 2008), and the 4TUd-labelled RNAs can be identified by thio-linked-biotinylation and streptavidin-affinity labelling or isolation. Thus, we generated a line of transgenic mice that expressed the *T. gondii* UPRT only in CMs, which enabled us to specifically label and track the miRs produced by endogenous CMs. Subsequent experiments confirmed that 4TUd incorporation was highly specific and sensitive for cardiac miRs, and that CM-derived miR-208a (^{CM}miR-208a) was evident in the lungs of intact mice. Furthermore, pulmonary ^{CM}miR-208a levels increased drastically in response to experimentally induced MI, and circulating sEV (^{PB}sEV) isolated from mice after MI significantly downregulated the expression of miR-208-targeted genes, while increasing the expression of endothelial adhesion molecules and the infiltration of pro-inflammatory cells, in mouse lungs. In contrast, pre-treatment of mice with anti-miR-208a attenuates MI-induced pulmonary miR-208a target gene downregulation, EC adhesion molecule expression, and inflammatory cell infiltration. Thus, CM-derived sEV and cargo miR-208a may contribute to MI-associated pulmonary inflammation.

2 | METHODS

2.1 | Animals

All animal experiments were approved by the Institutional Animal Care and Use Committee (IACUC) of the University of Alabama at Birmingham (UAB), and comply with all relevant ethical regulations, including the National Institutes of Health (NIH) "Guide for the Care and Use of Laboratory Animals". Experiments were conducted in 8–10 week-old male C57BL/6J mice unless specified otherwise. Mice were fed ad libitum and maintained in a climate-controlled facility (22°C, 43% humidity) with a 12:12-h light:dark cycle. Two transgenic mouse lines, B6;D2-Tg (CAG-GFP,-Uprt)985Cdoe/J (i.e., CA-GFPstop-HA-UPRT or GFPstop^{fl}-UPRT mice) (Gay et al., 2013) and B6.FVB-Tg(Myh6-cre)2182Mds/J (i.e., ^{CM}Cre mice) (Agah et al., 1997) were purchased from the Jackson Laboratory and bred to generate mice with CM-specific expression of the *T. gondii* UPRT (^{CM}UPRT mice). All offspring were genotyped via PCR for 35 cycles with appropriate primers (Table S1); each cycle consisted of 20 s at 95°C, 30 s at 57°C, and 20 s at 72°C.

2.2 | MI induction and sham surgery

Myocardial infarction induction and sham surgery were performed as previously described (Gao et al., 2010). Briefly, mice were anesthetized with isoflurane (2-4%), the heart was displaced via a left intercostal thoracotomy, and MI was induced via permanent ligation with a 6-0 silk suture placed 2 mm below the origin of the left anterior descending coronary artery (LAD); then, the heart was repositioned in the thoracic cavity, air was evacuated, and the chest was closed. The sham operated animals underwent all surgical procedures for MI induction except LAD ligation. After surgery, the animal remained on the heating pad to maintain body temperature, and heart and respiratory rates were continuously monitored until the animal was sternal and fully ambulatory and regained toe-pinch reflex. Pain control was provided via subcutaneous injections of buprenex (0.05 mg/kg) and carprofen (5 mg/kg) immediately after surgery; if mice were maintained for more than 12 h, buprenex (0.05 mg/kg) was readministered every 12 h for 48 h, and carprofen (5 mg/kg) was readministered once daily for 3 days.

2.3 | 4TUc administration

4TUc stock solution was prepared by dissolving 200 mg of 4TUc (catalogue #440736, sigma, St. Louis, MO, USA) in 1 ml of dimethyl sulfoxide (DMSO) and stored away from light. Immediately before injection, the stock solution was diluted with corn oil to a final concentration of 50 mg/ml and vigorously vortexed; then, the solution was administered via intraperitoneal injection (400 mg/kg per mouse). For analyses in intact mice, animals were injected once 6 h before euthanasia and tissue collection. Animals that underwent MI-induction or sham surgery received one dose 12 h before the surgical procedure and a second dose immediately afterward.

2.4 | ^{PB}sEV isolation and injection

Blood was drawn into collection tubes containing ethylenediaminetetraacetic acid (EDTA) and centrifuged at 500 g for 10 min; then, the supernatant was collected and centrifuged at 3000 g for 15 min to remove platelets. The platelets-depleted plasma was diluted 1:20 in ice-cold PBS and centrifuged at 15000 g and 4°C for 40 min, then the supernatant was filtered through a PES filter of 0.22 μm pore size (Millipore) and ultracentrifuged at 120,000 g for 2 h (Sorvall WX80 S/N: 761380; Thermo Fisher Scientific, Waltham, MA, USA). The pellets were resuspended in ice-cold PBS and ultracentrifuged again at 120,000 g for 2 h. The ^{PB}sEV in the pellets were resuspended in ice-cold PBS for further use. The protein concentrations were measured with a Pierce BCA Protein Assay Kit (catalogue #23225, Thermo fisher Scientific, Waltham, MA, USA). MI- and Sham-^{PB}sEV were obtained 12 h after MI or sham surgery, respectively, and administered to intact mice (100 μg ^{PB}sEV in 100 μl PBS) via two intravenous injections performed 24 h apart.

2.5 | miR-208a antagomir synthesis and administration

The miR-208a antagomir (LNA-anti-miR-208a) and control (LNA-anti-*Caenorhabditis elegans* cel-miR-67) oligonucleotides (*C*TTT*TT*G*C*T*CG*T*C*T*TA* and *T*CC*TA*G*AA*A*GA*GT*AG*A, respectively, with the LNA-modified nucleotides displayed in underlined, italicized font) were synthesized at Integrated DNA Technologies (Coralville, Iowa, USA). LNA-anti-miR-208a was complementary to the 5′ region of the mature miR-208a sequence and potently silences miR-208a for 2 weeks when

administered at 25 mg/kg (Montgomery et al., 2011). The antagomir or control oligonucleotide was injected into the tail-vein (25 mg/kg in 100 μl PBS per mouse) immediately before AMI induction or sham-AMI surgery.

2.6 | RNA purification and thiolated RNA isolation

Thiolated RNAs were protected from light at all times. The isolation and purification protocols have been described previously (Gay et al., 2014). Briefly, tissues or ^{PB}sEV were homogenized in 1 ml TRIzol (Thermo Fisher Scientific) with a TissueRuptor (Qiagen, Germantown, MD, USA) and extracted with 200 μl chloroform; then, total RNA was precipitated from the aqueous phase via the addition of glycogen, Dithiothreitol (DTT), and 0.5 ml cold isopropanol, followed by centrifugation at 12,000 g and 4°C for 10 min. The RNA-containing pellets were rinsed with 75% ethanol and centrifuged at 12,000 g and 4°C for 5 min; then, the supernatant was removed, the pellet was dissolved in RNase-free water, and RNA concentration and purity were determined via Nanodrop (Thermo Fisher Scientific).

Ribosomal RNAs (rRNAs) were removed with a RiboMinus Transcriptome Isolation Kit (Thermo Fisher Scientific); then, the rRNA-free RNAs were reacted with EZ-Link biotin-HDPD (Thermo Fisher Scientific), purified with an RNeasy minikit, and eluted in 20 μl of RNase-free water. Biotinylated RNAs were isolated with a μMacs streptavidin kit (Miltenyi Biotec, Waltham, MA, USA) as directed by the manufacturer's instructions, but with 2-mercaptoethanol (100 mM) rather than DTT used for the elution step, and then purified via ethanol precipitation.

2.7 | Dot blot analysis

Dot blot analysis was performed by following published protocols (Rädle et al., 2013; Sharma et al., 2018). Briefly, RNA was applied with a biotin-labelled DNA oligonucleotide (positive control; Integrated DNA Technologies) to a BrightStar-Plus positively charged nylon membrane (Thermo Fisher); then, the membrane was air-dried at room temperature for 5 min, blocked with 10% sodium dodecyl sulphate (SDS) in PBS and 1 mM EDTA at room temperature for 30 min, incubated in 10% SDS/PBS with HRP-conjugated streptavidin (Thermo Fisher Scientific) at room temperature for 15 min, and washed for 5 min with each of three progressively declining concentrations of SDS (10%, 1%, and 0.1%) in PBS. Biotinylated RNAs were detected with ECL Prime Western Blotting detection reagent (GE Healthcare Life Sciences, Chicago, IL) and a ChemiDoc MP Imaging System (Bio-rad, Hercules, California, USA).

2.8 | Quantitative real-time polymerase chain reaction (qPCR)

For analysis of mRNA abundance, RNA was reverse-transcribed with PrimeScript Reverse Transcriptase (catalogue #2680A, Takara, Kusatsu, Shiga, Japan), and then qPCR was performed with Fast SYBR Green Master Mix (catalogue #4385610, Thermo Fisher Scientific) and appropriate primer sequences (Table S1). Measurements were normalized to the abundance of GAPDH mRNA. For analysis of miR abundance, qPCR was performed as described previously (Sharma et al., 2016) with pre-designed assays for mouse miR-1a-3p, miR-133a-3p, miR-499-5p, miR-208a-3p, miR-122-5p, miR-192-5p, miR-195a-3p, and cel-miR-39-3p (Life Technologies). For quantifying cellular miRs, measurements were normalized to the abundance of U6 small nuclear RNA (internal control). For quantifying 4TUd-labelled miRs, Cel-miR-39 standard was included as an external reference in an amount equal to isolated 4TUd-incorporated RNA (1–10 ng) and used for normalization. For quantifying miRs in ^{PB}sEV, a group of six miRNAs (miR-19b-3p, 103-3p, 154–5p, 200b-3p, 342–3p, and 434-3p; hereto collectively referred as "$^{PB\text{-}Stable}$miRNAs") we have previously identified to have best stability measures in the circulation and not to be affected by MI (Cheng et al., 2019) were used as reference. The relative mRNA/miRNA expression level for each gene/miRNA was calculated via the $2^{(-\Delta\Delta Ct)}$ method. ΔCt = Ct (gene/miRNA of interest) – Ct (housekeeping gene/control reference) [Ct is $(Ct_{miR19b} + Ct_{miR103} + Ct_{miR154} + Ct_{miR200b} + Ct_{miR342} + Ct_{miR434})$ / 6 when normalized to $^{PB\text{-}Stable}$miRNAs], $\Delta\Delta Ct = \Delta Ct$ (experimental sample) – ΔCt (control sample), and the relative expression value equals power (2, $-\Delta\Delta Ct$).

2.9 | RNA sequencing analysis

Small RNA library was prepared with QIAseq miRNA Library Kit following manufacturer's instructions. Briefly, total RNAs were isolated from ^{PB}sEV, then subjected sequentially to 3′ and 5′ adapter ligations (sequence-3′ adapter AACTGTAGGCACCATCAAT and 5′ adapter GTTCAGAGTTCTACAGTCCGACGATC), cDNA synthesis and cDNA library pre-amplification, followed by high-throughput sequencing on an NextSeq500 (single end 75 bp mode). For informatics analysis of miRNA abundance, the 3′ adapter sequence and low-quality bases were removed using cutadapt (cutadapt.readthedocs.io/en/stable/guide.html), and the sequence was analysed in GeneGlobe Data Analysis Centre provided by QIAGEN with no spike-ins and 1 lane option.

2.10 | Isolation of hematopoietic, endothelial, and epithelial cells from lung tissue

Hematopoietic, endothelial, and epithelial cells were isolated via immunoaffinity for the corresponding cell-type specific surface markers (CD45, CD31, and CD326, respectively) (Nakano et al., 2018). Briefly, lung tissue was perfused with PBS; cut into small pieces; and digested with RPMI medium containing 4 U/ml elastase, 1 U/ml dispase, and 200 μg/ml DNase for 45 min at 37°C. Isolated cells were passed through a 70-μm cell strainer; any remaining pieces of undigested tissue were digested with RPMI containing 25 μg/ml Liberase and 200 μg/ml DNase for 30 min at 37°C and passed through a 70-μm cell strainer to collect more cells. Then, all cells were combined into a single solution, precipitated by centrifugation, resuspended in PBS, and incubated with biotinylated anti-CD45 antibody. Hematopoietic ($CD45^+$) cells were collected with streptavidin-coated magnetic beads, and cells that remained in the flow-through were precipitated, resuspended (1×10^8 cells/ml) in flow-cytometry buffer (0.5% bovine serum albumin [BSA], 0.1% NaN_3, and 2 mM EDTA in PBS), and incubated with allophycocyanin-conjugated anti-CD31 antibodies and phycoerythrin-conjugated anti-CD326 antibodies; then, endothelial ($CD31^+$) and epithelial ($CD326^+$) cells were sorted with a BD FACSymphony Flow Cytometer.

2.11 | Isolation of bone marrow mononuclear cells (BM MNC)

BM cells were obtained by flushing the cavity of the femurs and tibias with PBS, and BM MNC were isolated via density centrifugation using 1.083 g/ml histopaque (MilliporeSigma, Cat#10831). Briefly, 15 ml BM cells were carefully layered onto 15 ml histopaque 1083, then centrifuged at 400 g and room temperature for 30 min. The BM MNC were carefully collected from the buffy coat and washed with PBS for three times before use.

2.12 | Nanoparticle tracking analysis (NTA)

^{PB}sEV were evaluated with a Nanosight NS300 instrument (Malvern Panalytical, Malvern, UK) in the UAB High-Resolution Imaging Facility. Settings were optimized and remained constant between samples, and each video was analysed to determine the mean, mode, median, and concentration for each particle size. Measurements were performed at 1:1000 to 1:2500 dilution, yielding particle concentrations of 10^6–10^8 particles/ml, as recommended by the manufacturer. Samples were analysed in triplicate.

2.13 | Transmission electron microscopy (TEM)

TEM was performed with an FEI Tecnai T12 transmission electron microscope in the UAB High-Resolution Imaging Facility. Freshly prepared ^{PB}sEV were placed on a copper grid coated with 0.125% Formvar in chloroform, the grid was stained with 1% v/v uranyl acetate in ddH_2O, and ultra-thin sections (65 nm) were stained with uranyl acetate and Reynold's lead citrate. Imaging was performed immediately after sample preparation.

2.14 | Fluorescence microscopy

Mice were perfused with PBS under deep anaesthesia. The heart, liver, spleen, lung, kidney, and skeletal muscles were harvested, fixed in 4% paraformaldehyde for 12 h, dehydrated in 20% sucrose solution, embedded in optimal cutting temperature (OCT) compound, and cut into frozen sections. Cell nuclei were stained with DAPI in antifade mounting media (Vector Laboratories, Burlingame, CA, United States) as directed by the manufacturer's instructions, and GFP fluorescence was observed with an Olympus IX83 microscope.

2.15 | Histology

After euthanasia, the lung bronchoalveolar lavage fluids were removed through a cut in the trachea (Barile et al., 2017), then the lung was perfused with O.C.T compound and freshly frozen (Ling et al., 2009). The lung, liver, spleen, kidney, and skeletal muscles were cut into 10-μm sections, which were subsequently fixed in 4% paraformaldehyde, washed once in PBS, treated with 0.05% Triton X-100, and blocked with 5% BSA. For CD45 immunohistochemistry (IHC) staining, the tissue sections were incubated with biotin-conjugated rat anti-mouse CD45 antibody (1:200 dilution; BD biosciences) and with HRP-conjugated streptavidin (1:200; catalogue #N100, Thermo fisher); and the protein was visualized with RAB substrate and Harris Haematoxylin

counterstaining. For CD68 immunofluorescence (IF) staining, the tissue sections were incubated with rabbit anti-CD68 antibody (1:100 dilution; eBiosciences) and with AF488-conjugated goat-anti-rat IgG (1:200 dilution; Thermo fisher); and then counterstained with DAPI. The sources and working concentrations of antibodies are reported in Table S2.

2.16 | Western blot

Proteins were extracted from mouse tissues or ^{PB}sEV with RIPA lysis buffer (25 mM Tris•HCl pH 7.6, 150 mM NaCl, 1% NP-40, 1% sodium deoxycholate, 0.1% SDS) (Thermo fisher); denatured with 4 x Laemmli buffer (Bio-rad) containing 10% 2-mercaptoethanol at 95°C for 5 min, separated via electrophoresis with a 12% SDS-polyacrylamide gel, and then transferred to a polyvinylidene fluoride (PVDF) membrane. The membrane was blocked with 5% nonfat milk, incubated with a primary antibody for hemagglutinin (HA), β-tubulin, α-MHC, cytochrome c, lamin A/C, CD36, CD63, CD81, CD9, TSG101, GAPDH, Tmbim6, or NLK, then with an anti-mouse HRP or anti-rabbit HRP secondary antibody (Table S2). Proteins were visualized with ECL Prime Western Blotting detection reagent on a ChemiDoc MP Imaging System. GAPDH abundance was used to control for unequal loading.

2.17 | Statistical analysis and reproducibility

Data are presented as mean ± standard deviation. Sample size calculations and statistical analyses were performed with Prism 5 software (GraphPad Software, La Jolla, CA, USA).

The normality of data was tested with the Shapiro-Wilk test. For the data with a normal distribution, significance was evaluated via the two-tailed *t* test for comparisons between two groups or via analysis of variance (ANOVA) with the post-hoc Newman-Keuls test for multiple comparisons. For the data with non-normal distributions, significance was evaluated via the non-parametric Mann Whitney test. For data with a sample size $n = 3$, the non-parametric test presented in (Bian et al., 2021) was applied; in this case, the null hypothesis is H0: the probability that a random (group-1 sample > group-2 sample) is 0.5. A *P*-value of less than 0.05 was considered significant. Western blotting was performed at least twice to confirm the similarity of results.

3 | RESULTS

3.1 | 4TUd is incorporated into newly transcribed CM-derived RNAs of ^{CM}UPRT mice

CA-GFPstop^{flox}-HA·UPRT (GFPstop^{fl}-UPRT) mice carry a floxed genetic sequence that codes for GFP expression and blocks expression of the downstream hemagglutinin (HA)-tagged *T. gondii* UPRT fusion protein. Thus, we generated a line of transgenic mice that express *T. gondii* UPRT specifically in CMs (^{CM}UPRT mice) by breeding GFPstop^{fl}-UPRT mice with mice that expressed Cre recombinase from the cardiac α myosin heavy chain (αMHC) promoter (^{CM}Cre mice) (Figure S1A). Subsequent assessments confirmed that GFP expression was knocked out (Figure 1A) and HA-UPRT expression was activated (Figure 1B-C) in the CMs of ^{CM}UPRT mice, but not in any other cardiac-cell type or organ (Figure S1B-C), and when cardiac RNA was isolated from mice 6 h after treatment with intraperitoneal injections of 4TUc, biotinylated, and labelled with streptavidin-conjugated horseradish peroxidase (HRP), the HRP signal was ~10-fold greater in RNAs from ^{CM}UPRT mice than from ^{CM}Cre mice (Figure 1D). HRP chemiluminescence was also much greater in cardiac RNAs from ^{CM}UPRT than from ^{CM}Cre mice after ribosomal RNAs, which comprise the bulk of the total cellular RNA content, had been depleted with Ribominus (Figure 1E), and in RNAs isolated from the peripheral-blood sEV (^{PB}sEV-RNAs) of ^{CM}UPRT mice than in ^{CM}Cre ^{PB}sEV-RNAs (Figure 1F). The HRP signals in cardiac and ^{PB}sEV RNAs from ^{CM}UPRT mice without 4TUc injection were negligible (Figure S2).

3.2 | ^{PB}sEV transport CM-derived miRs from the heart to the lung

The CM-specificity of miR labelling was also evaluated by comparing 4TUd incorporation in miRs that are predominantly expressed by CMs (miR-1, 133, and 208), skeletal muscle (miR-1 and 133), kidney (miR-499), hepatocytes (miR-122 and 192), lung (miR-195), spleen (miR-142), and brain (miR-9). In cardiac tissues, measurements of total (Figure 2A) and 4TUd-labelled (Figure 2B) RNA abundance were much greater for CM miRs than for kidney, hepatocyte, lung, spleen or brain miRs. Interestingly, the efficiency of 4TUd-labelling was greater for miR-208 than for miR-1 or -133 (Figure 2C), which could suggest that the rate of miR turnover was faster for miR-208 than for the other two CM miRs during the 6-h 4TUd-labelling period. ^{PB}sEV carried ample total amounts of cardiac miRs (miR-1, 133, and 208), as well as hepatic (miR-122), lung (miR-192), and spleen (miR-142)

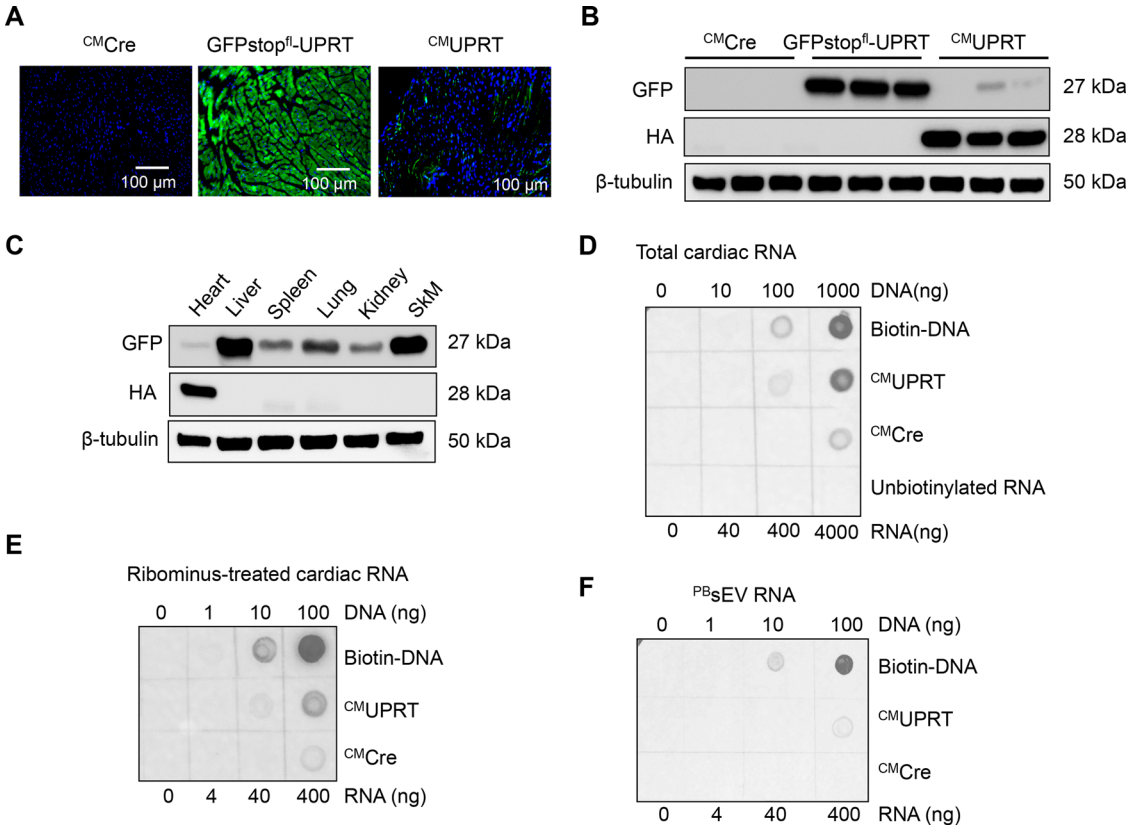

FIGURE 1 **4TUd is incorporated into newly transcribed CM-derived RNAs of ^{CM}UPRT mice.** Mice expressing *T. gondii* UPRTin CMs alone (^{CM}UPRT mice) were generated by breeding mice that expressed Cre recombinase from the CM-specific αMHC promoter (^{CM}Cre mice) with mice carrying a floxed genetic sequence that coded for GFP expression and blocked expression of the downstream hemagglutinin (HA)-tagged *T. gondii* UPRT (GFPstop^{fl}-UPRT mice). (**A**) Cre-mediated deletion of the floxed GFPstop sequence in ^{CM}UPRT mice was confirmed by comparing images of GFP fluorescence in the hearts of ^{CM}Cre, GFPstop^{fl}-UPRT, and ^{CM}UPRT mice. (**B-C**) GFP and HA protein abundance was evaluated in (**B**) the hearts of ^{CM}Cre, GFPstop^{fl}-UPRT, and ^{CM}UPRT mice and in (**C**) the heart, liver, spleen, lung, kidney, and skeletal muscle (SkM) of ^{CM}UPRT mice via Western blot; β-tubulin protein abundance was also evaluated to control for unequal loading. (**D–F**) RNA was isolated from (**D–E**) the hearts and (**F**) ^{PB}sEV of ^{CM}UPRT and ^{CM}Cre mice 6 h after the animals had been injected with 4TUc (400 mg/kg). (**D**) Total cardiac RNA, (**E**) Ribominus-treated cardiac RNA, and (**F**) total ^{PB}sEV RNA were biotinylated and labelled with HRP-tagged streptavidin to identify 4TUd-containing transcripts, and then the abundance of the HRP-labelled transcripts was evaluated via Dot blot. A biotin-labelled DNA oligonucleotide was included in the analysis to serve as a positive control.

miRs (Figure 2D), but substantial 4TUd incorporation and high efficiency of 4TUd-labelling (i.e., the ratio of 4TUd-labelled to total miR abundance) was only observed for cardiac miR-1 and miR-208 (Figure 2E-F), indicating robust 4TUd incorporation into CM-, but not other tissue-specific/enriched miRs. The ratio of 4TUd-labelled miR-133 to total miR-133 in ^{PB}sEV was lower than that of miR-1 and 208, which may reflect ^{PB}sEV miR-133 largely derived from skeletal muscles.

Total (Figure 2G) and 4TUd-labelled (Figure 2H) miR-208 (^{Total}miR-208 and ^{4TUd}miR-208, respectively) were also highly abundant in the lung, but not in the liver, kidney, bone-marrow mononuclear cells (BM MNC), or skeletal muscle, and the ratio of ^{4TUd}miR-208 abundance in the lung and heart (lung:heart = 1:200) was similar to the ratio of ^{Total}miR-208 in the same organs (lung:heart = 1:140), which suggests that much of the miR-208 present in the lung had been transported from the heart. Furthermore, when hematopoietic ($CD45^+$), endothelial ($CD31^+$), and epithelial ($CD326^+$) cells were isolated from lung tissues via immunoaffinity and fluorescence-activated single cell sorting (Figure S3), ^{4TUd}miR-208 was found in all three cell types and most abundant in ECs (Figure 2I). Collectively, these observations indicate that miR-208 was expressed in CMs and packaged into sEV, which were subsequently released into the peripheral blood and preferentially internalized by cells in the lungs, especially lung ECs.

3.3 | MI increases the abundance of CM-derived miR-208a in the lung

To determine whether MI alters the expression and distribution of CM-derived miR-208, assessments were conducted in mice that had been injected with 4TUc 12 h before and immediately after surgically induced MI or sham surgery. ^{PB}sEV collected 12 h after MI induction (MI-^{PB}sEV) or sham surgery (Sham-^{PB}sEV) were similar in size and morphology and contained equivalent

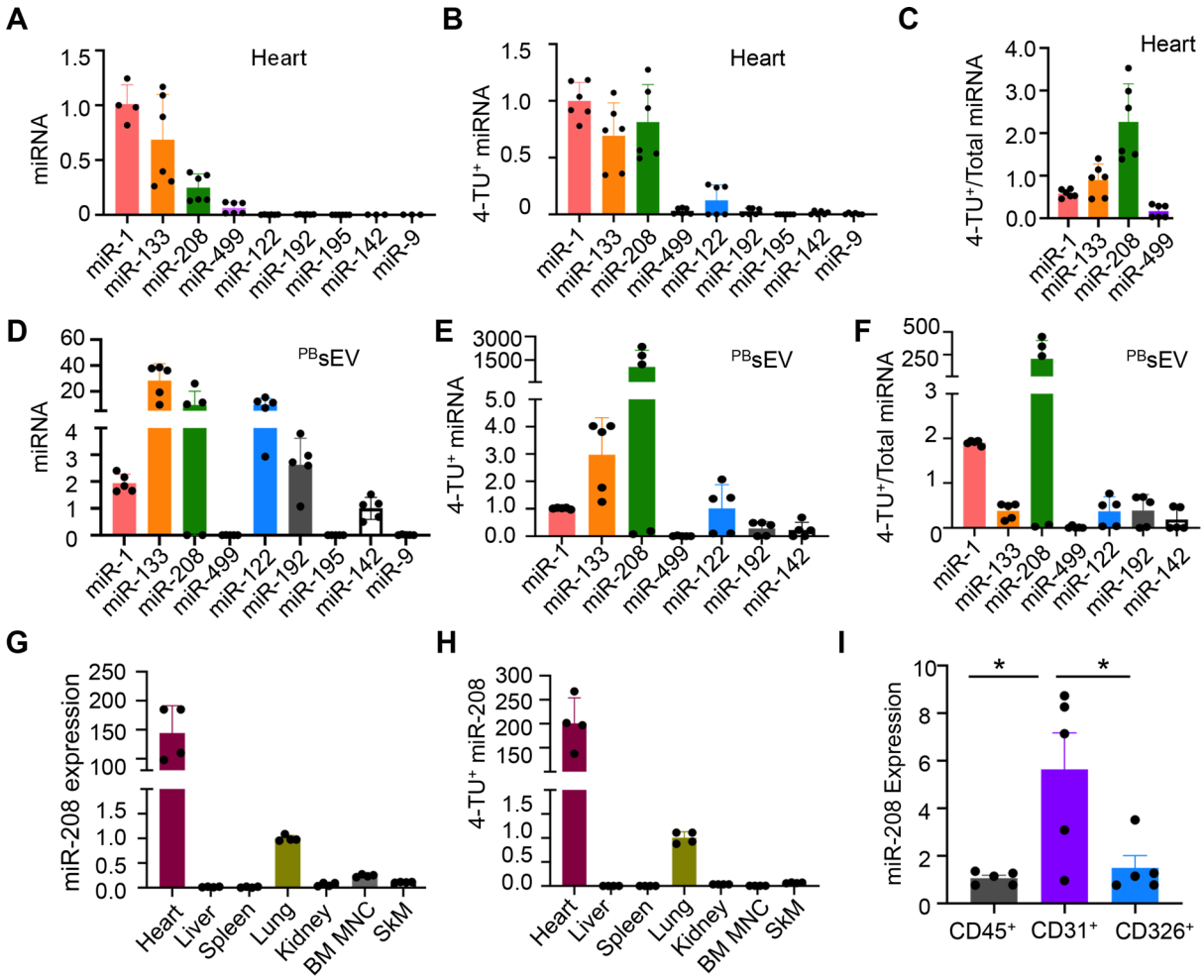

FIGURE 2 **^{PB}sEV transport CM-derived miRs from the heart to the lung.** Analyses were conducted in ^{CM}UPRT mice 6 h after 4TUc administration. (**A-F**) The abundance of transcripts for miRs that are predominantly associated with CMs (miR-1, 133, and 208), skeletal muscle (miR-1and 133), kidney (miR-499), hepatocytes (miR-122 and 192), lung (miR-195), spleen (miR-142), and brain (miR-9) was measured in (**A**) total, (**B**) 4TUd-containing RNA extracted from heart tissue and in (**D**) total, (**E**) 4TUd-labelled RNA collected from ^{PB}sEV. The ratios of 4TUd+/total RNA from heart (**C**) and ^{PB}sEV (**F**) were calculated. (**G-H**) The abundance of miR-208 was measured in (**G**) total and (**H**) 4TUd-containing RNA extracted from the heart, liver, lung, kidney, bone-marrow mononuclear cells (BM MNCs), and skeletal muscle (SkM). (**I**) miR-208 abundance was measured in the immunologically isolated lung CD45+, CD31+, and CD326+ cells. miR abundance was quantified via qPCR and normalized to U6 snRNA (A, G, and I), Cel-miR-39 (B, E, and H), or $^{PB\text{-}Stable}$miRNAs (D); data are expressed as mean ± standard deviation. $^*P < 0.05$. I, one-way ANOVA.

amount of TSG101 protein (Figure S4); however, the yield of MI-^{PB}sEV from each mouse was 38.5%, 25.2%, and 18.5% greater in protein, RNA, and particle accounts, respectively, than that of Sham-^{PB}sEV (Table S3), and MI-^{PB}sEV expressed higher levels of CD9, CD81, CD63, αMHC, and GAPDH markers and a lower level of β-actin protein (Figure S4). Bulk sequencing analysis identified numerous miRs that were differentially expressed in the two groups (Figure 3A), including miR-208, which was markedly enriched in MI-^{PB}sEV. When measured via quantitative polymerase chain reaction (qPCR), ^{4TUd}miR-208 abundance in ^{PB}sEV increased ~40-fold from before MI induction until 12 h afterward but was nearly undetectable at 48 h (Figure 3B), while ^{4TUd}miR-208 abundance in the lung peaked 24 h after MI induction (Figure 3C) and remained substantially higher than ^{4TUd}miR-208 levels in the kidney, liver, BM cells, or skeletal muscle (Figure 3C-D). Notably, miR-208a is expressed from intron 29 of the αMHC gene, but αMHC mRNA was nearly undetectable in the lung (Figure 3D), which confirms that the MI-induced increase in ^{4TUd}miR-208 abundance was not caused by the activation of αMHC expression in lung cells.

3.4 | CM-derived miR-208 downregulates NLK and Tmbim6 expression and upregulates pro-inflammatory response in the lung

miR-208 targets nemo-like kinase (NLK) and transmembrane BAX inhibitor motif containing 6 (Tmbim6) (Figure S5) (Montgomery et al., 2011; Wilkes et al., 2021; Yan et al., 2016). Thus, we compared the expression of these two miR-208 targets in the

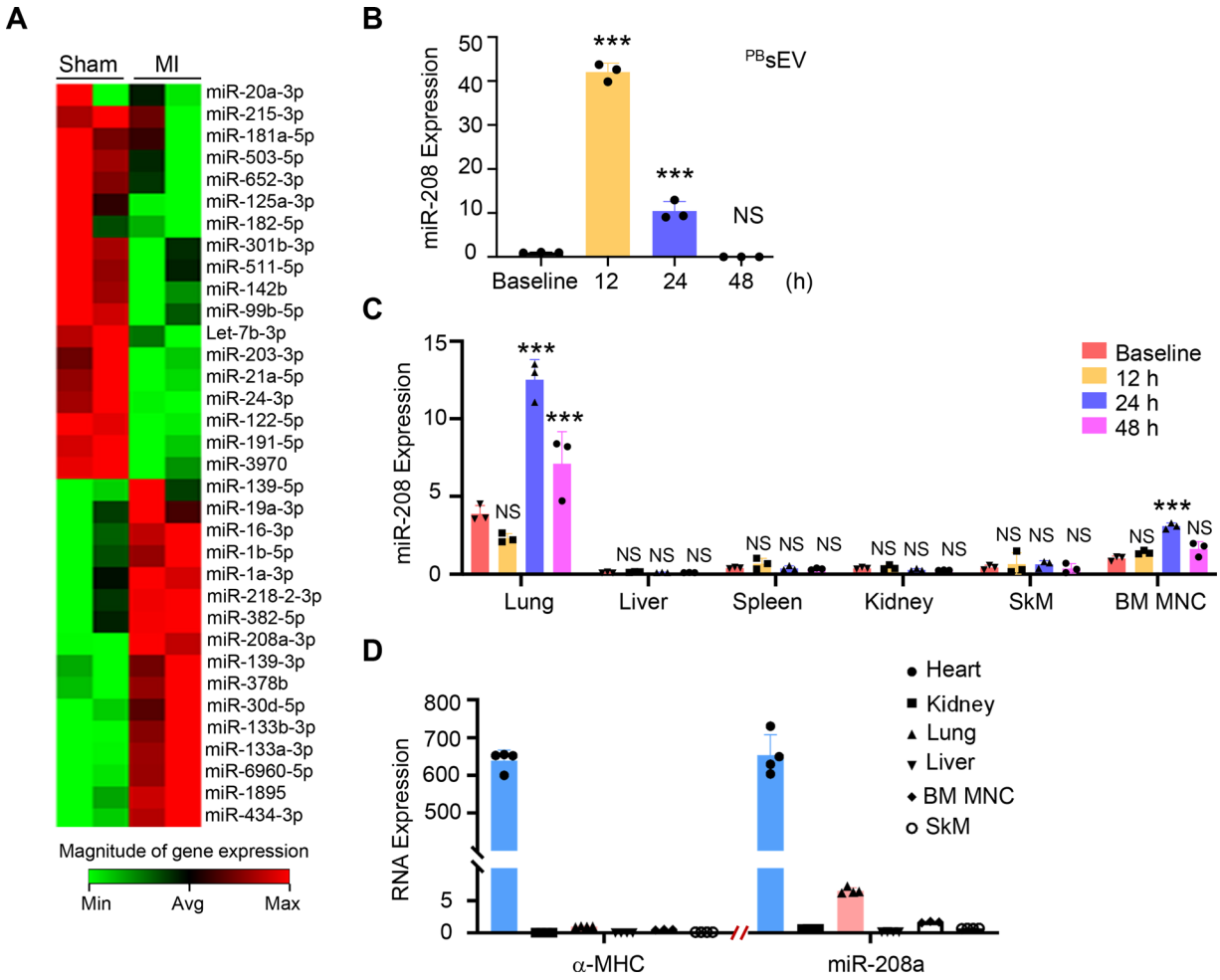

FIGURE 3 **MI increases the abundance of CM-derived miR-208a in the lung.** ^{CM}UPRT mice were injected with 4TUc 12 h before and immediately after surgically induced MI or sham surgery. (**A**) miR abundance was determined via bulk sequencing analysis in ^{PB}sEV collected 12 h after MI induction or sham surgery ($n = 2$). (**B–C**) The abundance of miR-208a transcripts was determined (**B**) in ^{PB}sEV and (**C**) in tissues from the lung, liver, spleen, and kidney, in skeletal muscle (SkM) tissues, and in bone-marrow mononuclear cells (BM MNC) collected before MI induction and 12, 24, and 48 h afterward ($n = 3$). ***$P < 0.001$; NS, not significant versus baseline. One-way ANOVA. (**D**) The abundance of αMHC and miR-208a transcripts was determined in tissues from the heart, kidney, lung, and liver, in SkM tissues, and in BM MNC collected 24 h after MI induction ($n = 4$). Measurements in panels B, C, and D were performed via qPCR and normalized to $^{PB\text{-}Stable}$miRNAs (B), U6 snRNA (C and *right* panel of D), or GAPDH mRNA (*left* panel of D).

lungs of intact mice 24 h after the animals had received intravenous injections of 100 μg of MI- or Sham-^{PB}sEV, constituting 308 ng or 338 ng RNA, respectively; a third group of animals was injected with an equivalent volume of PBS alone. Compared to the PBS control, injection of MI-^{PB}sEV led to 2.3 fold increase in the level of lung miR-208a, whereas injection of Sham-^{PB}sEV did not change lung miR-208a level significantly (Figure 4A). NLK mRNA abundance did not differ significantly among the three groups (Figure 4B). NLK protein levels were similar in animals treated with Sham-^{PB}sEV and PBS but significantly lower in MI-^{PB}sEV– than in Sham-^{PB}sEV– or PBS-treated animals (Figure 4C). Both Tmbim6 mRNA and protein levels were similar in PBS- and Sham-^{PB}sEV–injected animals but declined in response to MI-^{PB}sEV injection (Figure 4B-C).

NLK and Tmbim6 also suppress the activity of multiple proteins that participate in nuclear factor kappa B (NF-κB) signalling pathway (Huang et al., 2016; Lisak et al., 2016; Liu et al., 2015; Yasuda et al., 2004), which regulates inflammation, and mRNA levels for downstream targets of the NF-κB pathway, including intercellular adhesion molecule 1 (ICAM-1), vascular cell adhesion molecule 1 (VCAM-1), and E-selectin, were greater in the lungs of MI-^{PB}sEV animals than in lungs from the Sham-^{PB}sEV or PBS group (Figure 4D). MI-^{PB}sEV treatment of human vein endothelial cells (HUVECs) for 12 h led to more nuclear phospho-p65 protein (i.e., activated NF-κB) than Sham-^{PB}sEV treatment (Figure S6). Notably, the upregulated expression of ICAM-1, VCAM-1 and E-selectin in the lung of MI-^{PB}sEV animals was associated with increased alveolar wall thickness (Figure 4E), collagen content (Figure S7), and numbers of infiltrating hematopoietic (CD45+) cells and monocytes/macrophages (CD68+) (Figure 4F-G & Figure S8A-B). Interestingly, mRNA levels of NLK, Tmbim6, ICAM-1, VCAM-1, and E-selectin (Figure S9) and numbers of infiltrating CD45+ and CD68+ cells (Figure S10-11) in the liver, kidney, spleen, skeletal muscles, and BM MNC were similar between the three groups, except for slightly decreased liver and kidney Tmbim6 expression and slightly increased liver CD45+ cells in MI-^{PB}sEV treated animals (Figures S9-11). When an miR-208 antagomir or control oligonucleotide was

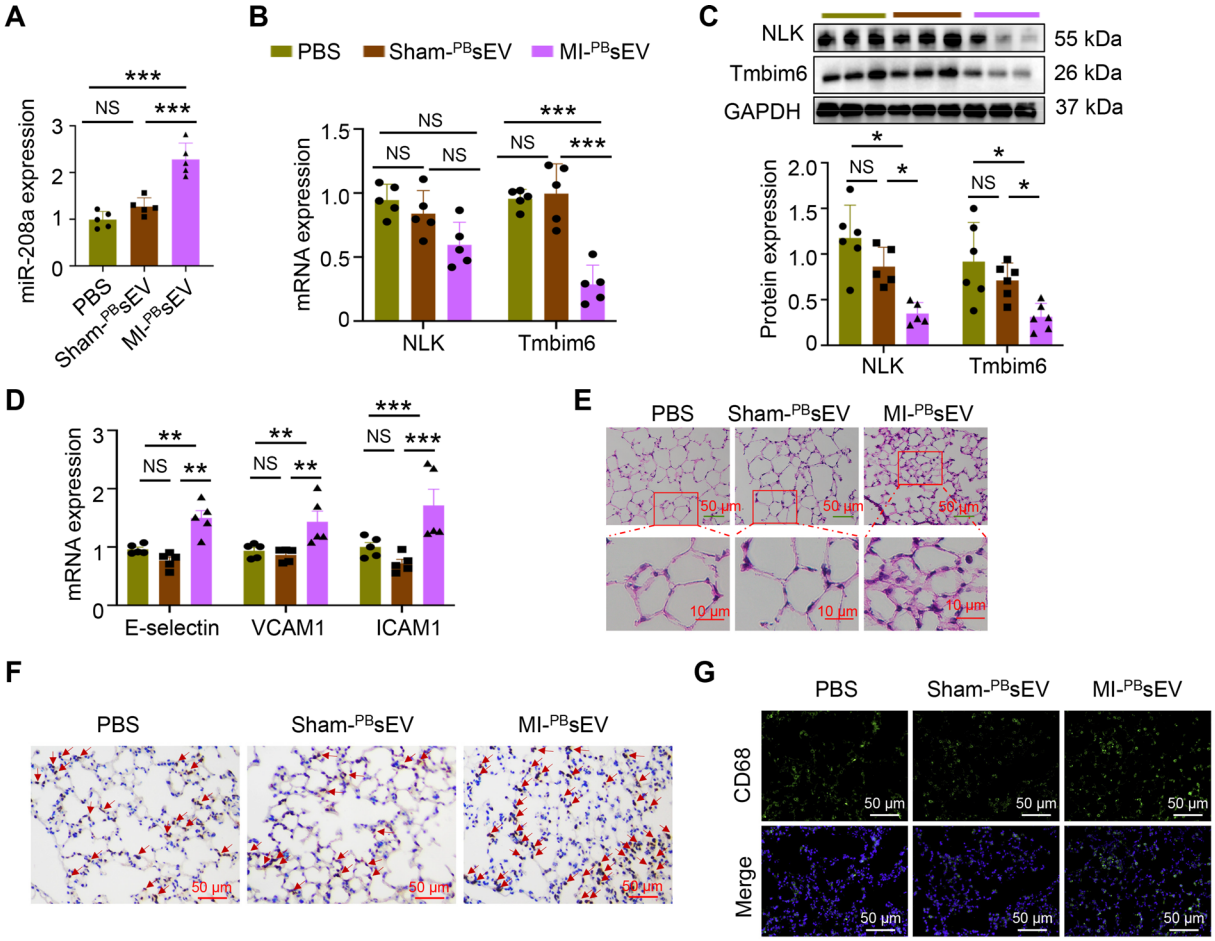

FIGURE 4 **Administration of exogenous MI-^{PB}sEV downregulates NLK and Tmbim6 expression and induces pro-inflammatory response in the lung of uninjured mice.** ^{PB}sEV were collected from mice 12 h after MI induction (MI-^{PB}sEV) or sham surgery (Sham-^{PB}sEV) and then intravenously injected into uninjured mice; ^{PB}sEV were delivered in two doses administered 24 h apart, and a third group of uninjured mice was injected with equivalent volumes of PBS. The lung tissues were harvested 24 h after the second dose and evaluated for the expression levels of (**A**) miR-208a; (**B-C**) NLK and Tmbim6 mRNA (**B**) and protein (**C**); and (**D**) E-selectin, VCAM-1, and ICAM-1 mRNA; as well as the (**E**) thickness of alveolar walls (H&E staining); and (**F–G**) numbers of infiltrating CD45+ hematopoietic cells (**F**) and CD68+ monocyte/macrophages (**G**). Data are reported as mean ± standard deviation (n = 5–6). Measurements in panels A, B, and D were performed via qPCR and normalized to U6 snRNA (A) or GAPDH mRNA (B and D). $^{*}P < 0.05$, $^{**}P < 0.01$, $^{***}P < 0.001$. NS, not significant. A: one-way ANOVA; B and lower panel of C: two-way ANOVA; and D: Mann-Whitney test.

co-administered with MI-^{PB}sEV, the MI-^{PB}sEV–induced downregulation of NLK and Tmbim6 and increase in CD45^{+} and CD68^{+} cell infiltrations in the lung were diminished by miR-208a antagomir co-treatment, but not by control oligo co-treatment (Figure S12A-C).

Furthermore, we evaluated the physiological effect of the elevated heart-to-lung miR-208 transfer in injured animals. miR-208 levels in the lung were significantly lower 3 days after MI was induced in mice that had received intravenous injections of an LNA-modified miR-208 antagomir, rather than a control antagomir sequence, immediately before MI surgery (Figure 5A), and pretreatment with the miR-208 antagomir increased NLK and Tmbim6 mRNA and protein levels (Figure 5B-C), while reducing the abundance of ICAM1, VCAM1, E-selectin, TNF-α, and IL-1β mRNA expression (Figure 5D), alveolar wall thickness (Figure 5E), collagen content (Figure S13), and hematopoietic and monocyte/macrophage infiltrations (Figure 5F-G & Figure S14A-B), in the lungs on Day 3 after MI. Notably, neither MI surgery nor miR-208 antagomir pretreatment significantly altered NLK and Tmbim6 mRNA and protein levels in the liver, kidney, spleen, SkM, or BM MNC (Figure S15). Thus, CM-derived miR-208 appears to target NLK and Tmbim6 in the lung where it promotes the inflammatory response to MI.

4 | DISCUSSION

miRs are key regulators of numerous cellular processes that maintain physiological homeostasis and can contribute to disease; however, an adequate understanding of these regulatory mechanisms can only be gained through the use of techniques that can

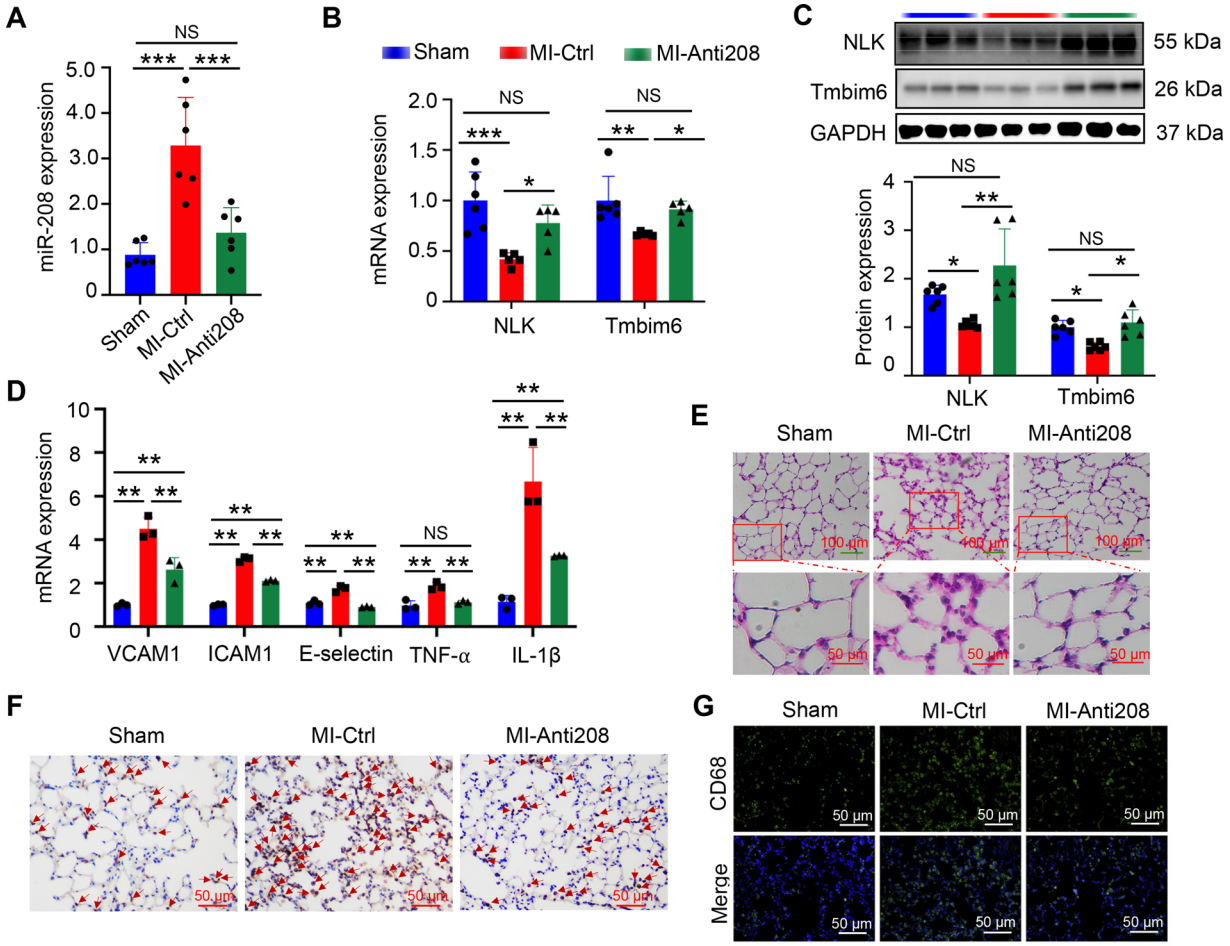

FIGURE 5 **CM-derived miR-208 downregulates NLK and Tmbim6 expression and upregulates inflammation in the lung of MI mice**. Mice were intravenously injected with an miR-208a antagomir (LNA-anti-miR-208a, 25 mg/kg) or a control (scrambled) oligonucleotide (Ctrl oligo, 25 mg/kg) before MI induction; a third group of mice underwent sham surgery without receiving the antagomir or control oligonucleotide. The lung tissues were harvested 3 days after MI induction or sham surgery and evaluated for the expression levels of (**A**) miR-208a; (**B–C**) NLK and Tmbim6 mRNA (**B**) and protein (**C**); and (**D**) VCAM-1, ICAM-1, E-selectin, TNF-α and IL-1β mRNAs; as well as the (**E**) thickness of alveolar walls (H&E staining); and (**F-G**) numbers of infiltrating CD45+ hematopoietic cells (**F**) and CD68+ monocyte/macrophages (**G**). Data are reported as mean $\pm$ standard deviation. $n = 3–9$. Measurements in panels A, B, and D were performed via qPCR and normalized to U6 snRNA (A) or GAPDH mRNA (B and D). $^*P < 0.05$, $^{**}P < 0.01$, $^{***}P < 0.001$. NS, not significant. A, B, lower panel of C, and D: Mann-Whitney test.

accurately track the sEV-mediated transfer of miRs between organs. Here, we show that when our newly generated ^{CM}UPRT mice were injected with 4TUc, 4TUd was incorporated into ^{CM}miRs with high specificity and sensitivity, and that the 4TUd-containing ^{CM}miRs could be efficiently biotinylated and labelled with fluorescent streptavidin conjugates or captured with streptavidin-conjugated beads. We also demonstrated that ^{CM}miR-208a was packaged into ^{CM}sEV, which circulated in the peripheral blood until they were taken up by cells in the lungs, where their ^{CM}miR-208a cargo suppressed the expression of genes involved in NF-κB signalling. Thus, the results presented here are the first to identify an miR-mediated mechanism by which the heart can regulate gene expression in the lung.

The activity of miR-208 within CMs has been well-documented and includes roles in processes that contribute to cell growth, hypertrophy, electronic physiology, hormonal signalling, and energy metabolism (Callis et al., 2009; Grueter et al., 2012; van Rooij et al., 2007). However, the results presented here are the first to conclusively demonstrate that a substantial proportion of the miR-208 transcripts present in lung tissue, especially lung ECs, was transcribed in CMs. We also show that miR-208a suppresses the expression of inflammatory regulators (NLK, and Tmbim6) (Lisak et al., 2016; Yasuda et al., 2004; Zhang et al., 2018) while upregulating cell-adhesion molecules (ICAM-1, VCAM-1, and E-selectin) in the lung, which suggests that ^{CM}miR-208 may have a key role in several of the pulmonary complications associated with MI, such as edema, fibrosis, and the thickening of alveolar walls, which can contribute to the development of pulmonary hypertension and heart failure. Notably, NLK also regulates the proliferation of lung epithelial cells (Ke et al., 2016) and Tmbim6 is involved in the ER stress response; thus, ^{CM}miR-208a could have a role in many processes that contribute to MI-associated pulmonary remodelling.

NLK regulates the proliferative growth of the lung, and loss of NLK leads to smaller and compressed alveoli but thicker and hyperplastic mesenchyme, which are similar to changes occurred after acute MI (Ke et al., 2016). Importantly among the various functions shared by these two proteins is the repression of NF-κB expression and translocation into nucleus, thus pro-inflammatory response (Lisak et al., 2016; Yasuda et al., 2004; Zhang et al., 2018). Our more recent data reveal that treatment of MI-^{PB}sEV also led to increased expression of ICAM1, VCAM1, and E-selection in HUVECs in vitro. The significantly increased hematopoietic ($CD45^+$) and pro-inflammatory ($CD68^+$) cells further reveals the induced EC inflammation in lung after treatment with MI-^{PB}sEV or after MI. Indeed, deteriorated structural remodelling of the lungs and collagen accumulation in lung is observed after MI in our study, which is consistent with collagen and reticulin deposition, thickening of the alveolar septa and proliferation of myofibroblasts after MI shown in previous study (Jasmin et al., 2004; Jasmin et al., 2003). Thus, the increasing inflammatory cells and factors in early stage, as well as the subsequent induced myofibroblasts contribute to the MI induced serious lung remodelling. Collectively, our data and the results published from other laboratories strongly suggest that the ^{CM}miR-208a transfer may contribute to the functional remodelling of the lung after MI injury.

Myocardial infarction can affect the functional states of multiple remote organs (Aber et al., 1966; Burkhardt et al., 2010; Efendigil et al., 1975; Hirooka, 2010; Tang et al., 2018; Thackeray et al., 2018; Werner et al., 2021), however, ^{PB}sEV-derived ^{CM}miR-208a is predominantly enriched in the lung. The underlying mechanism is currently unknown and may involve preferential lodging, receptors-mediated targeting and internalization, or specific miR-208a half-life kinetics in acceptor cells (Kang et al., 2021; van Rooij et al., 2007). Systemic reviews on all source EV administered to animals suggest liver and lung the top two organs for EV enrichment (Kang et al., 2021), though most studies used modified EV to facilitate in vivo tracking, thus may have already altered their tissue tropisms (Han et al., 2022). Nevertheless, it should be noted that CM-^{PB}sEV–mediated selective enrichment of ^{CM}miR-208a in the lung does not indicate CM-^{PB}sEV are only specifically targeted to or captured in the lung. In fact, EV released from infarcted heart have shown to be endocytosed by infiltrating monocytes, leading to elevated local pro-inflammatory response (Loyer et al., 2018), and our lab has reported previously – and confirmed in this current study – that ischemic CM-^{PB}EV also transfer miR-208a into BM MNC, contributing to BM progenitor cell mobilization (Cheng et al., 2019). Intriguingly in BM MNC, the ^{CM}miR-208a level was also elevated after MI induction or MI-^{PB}sEV injections, but NLK and Tmbim6 expression were not downregulated. Whether this was due to the peak level of ^{CM}miR-208a that was substantially lower than that in the lung or to the lack of cellular environment required for miR-208a activation remains to be elucidated.

We have focused on miR-208a-3p rather than miR-208a-5p, as our miRNA-seq analyses reveal miR-208a-3p abundantly expressed in Sham-^{PB}sEV and markedly elevated in MI-^{PB}sEV, whereas miR-208a-5p is almost undetectable in both Sham-^{PB}sEV and MI-^{PB}sEV. These results are consistent with the observation that miR-208a-3p strand is overly dominant in the heart (Grueter et al., 2012; van Rooij et al., 2007). In addition, miR-208a and miR-208b share same seed sequence, thus molecular targets (Babiarz et al., 2012), and are both found to markedly increase in PB after acute MI (Liu et al., 2017); however, we did not detect miR-208b in MI-^{PB}sEV or lungs of mice. While miR-208a is transcribed from intron 29 of Myh6 (α-MHC) gene, miR-208b is expressed from intron 31 of Myh7 (β-MHC) gene (Callis et al., 2009; van Rooij et al., 2009). Unlike in adult humans where α-MHC expression is restricted to atrial CMs (Cui et al., 2019), α-MHC in adult rodents appears to be the predominant isoform in both atrial and ventricular CMs (Lompre et al., 1984; Tardiff et al., 2000). Interestingly, miR-208b is also expressed in SkM (Callis et al., 2009; van Rooij et al., 2009) and shown to regulate SkM development, metabolism, phenotypic switch, and injuries (Fu et al., 2020; Horak et al., 2016; Li et al., 2022; Wang et al., 2019; Zilahi et al., 2019). Outstanding questions, such as if the lack of miR-208b in mouse MI-^{PB}sEV is due to its low-level expression in the adult mouse heart or to its ineffective sorting into CM-^{PB}sEV, and whether miR-208b is carried in human CM- or SkM-derived ^{PB}sEV to influence the inflammatory state of lungs, remain to be addressed in the future.

In this study, we have also detected a low level of 4TUd incorporation in miR-122. miR-122 is one of the most abundant miRNAs in the liver, accounting for 70% and 52% of the whole hepatic miRNome in adult mice and humans, respectively (Bandiera et al., 2015). However, there are also reports suggesting that miR-122 can be expressed in ECs, vascular smooth muscle cells (VSMCs), CMs, cardiac fibroblasts (CFs), and adipocytes (Lunney et al., 2020; Rivoli et al., 2017; Song et al., 2020; Xu et al., 2016). Whether the low-level labelling of miR-122 was resulted from its expression in CMs or from a potential leak in our labelling system remains to be elucidated in our future studies.

In conclusion, our newly developed line of ^{CM}UPRT mice, which express the *T. gondii* UPRT only in CMs, enables us to track the sEV-mediated transport of CM-derived miRs. Studies conducted with these mice demonstrated that a substantial proportion of the miR-208 transcripts present in the lung was generated in CMs, that pulmonary levels of ^{CM}miR-208 increased in response to MI, and that miR-208 suppresses the expression of inflammatory regulators in lung cells. Thus, the experiments reported here are the first to identify an miR-mediated mechanism by which myocardial injury can alter the expression of genes in the lung, and that ^{CM}miR-208 may contribute to the pulmonary complications associated with MI.

ACKNOWLEDGEMENTS

We thank Dr. Mary Flowers Braswell for her generous donation of the Vevo 2100 VisualSonics Fujifilm Imaging System. This work was supported by the National Institute of Health (Grants# HL138990, HL131110, and HL113541 to Gangjian Qin); American

Diabetes Association (Grant# 1-15-BS-148 to Gangjian Qin); American Heart Association (Grant# 19TPA34910227 to Gangjian Qin; 19IPLOI34760713 to Junjie Yang, and 830472 to Chaoshan Han); (Methodology to Jianyi Zhang).

AUTHOR CONTRIBUTIONS

Chaoshan Han and G.Q. conceptualized the study, interpreted data and wrote the manuscript. Chaoshan Han performed most of the experiments and statistical analyses. Junjie Yang, Eric Zhang, Ying Jiang, Aijun Qiao, Yipeng Du, Qinkun Zhang, Junqing An, Jiacheng Sun, and Meimei Wang assisted in experiments and data analysis. Thanh Nguyen assisted in statistical analysis. Hind Lal, Prasanna Krishnamurthy, and Jianyi Zhang made intellectual contributions and helped in data interpretations.

CONFLICT OF INTEREST

The authors declare no competing financial interest.

ETHICS STATEMENT

All animal experiments were approved by the Institutional Animal Care and Use Committee (IACUC) of the University of Alabama, Birmingham (UAB), and comply with all relevant ethical regulations, including the National Institutes of Health (NIH) "Guide for the Care and Use of Laboratory Animals".

DATA AVAILABILITY STATEMENT

The microRNA-seq data is accessible at Gene Expression Omnibus (accession number: GSE205405 [https://www.ncbi.nlm.nih.gov/geo/query/acc.cgi?acc = GSE205405]). All remaining data are included in the article and Supplementary Information file.

REFERENCES

Aber, C. P., Brunt, P. E., Jones, E. W., Richards, T. G., & Short, A. H. (1966). Liver function after myocardial infarction. *Lancet*, *1*, 1391–1393.[CrossRef].

Agah, R., Frenkel, P. A., French, B. A., Michael, L. H., Overbeek, P. A., & Schneider, M. D. (1997). Gene recombination in postmitotic cells. Targeted expression of cre recombinase provokes cardiac-restricted, site-specific rearrangement in adult ventricular muscle in vivo. *Journal of Clinical Investigation*, *100*, 169–179.[CrossRef].

Babiarz, J. E., Ravon, M., Sridhar, S., Ravindran, P., Swanson, B., Bitter, H., Weiser, T., Chiao, E., Certa, U., & Kolaja, K. L. (2012). Determination of the human cardiomyocyte mrna and mirna differentiation network by fine-scale profiling. *Stem Cells and Development*, *21*, 1956–1965.[CrossRef].

Baietti, M. F., Zhang, Z., Mortier, E., Melchior, A., Degeest, G., Geeraerts, A., Ivarsson, Y., Depoortere, F., Coomans, C., Vermeiren, E., Zimmermann, P., & David, G. (2012). Syndecan-syntenin-alix regulates the biogenesis of exosomes. *Nature Cell Biology*, *14*, 677–685.[CrossRef].

Bandiera, S., Pfeffer, S., Baumert, T. F., & Zeisel, M. B. (2015). Mir-122–a key factor and therapeutic target in liver disease. *Journal of Hepatology*, *62*, 448–457.[CrossRef].

Barile, L., Moccetti, T., Marbán, E., & Vassalli, G. (2017). Roles of exosomes in cardioprotection. *European Heart Journal*, *38*, 1372–1379.

Bei, Y., Chen, T., Banciu, D. D., Cretoiu, D., & Xiao, J. (2017). Circulating exosomes in cardiovascular diseases. *Advances in Experimental Medicine and Biology*, *998*, 255–269.[CrossRef].

Bian, W., Chen, W., Nguyen, T., Zhou, Y., & Zhang, J. (2021). Mir-199a overexpression enhances the potency of human induced-pluripotent stem-cell-derived cardiomyocytes for myocardial repair. *Frontiers in Pharmacology*, *12*, 673621.[CrossRef].

Biddle, T. L., Khanna, P. K., Yu, P. N., Hodges, M., & Shah, P. M. (1974). Lung water in patients with acute myocardial infarction. *Circulation*, *49*, 115–123.[CrossRef].

Burkhardt, R., Toh, S. A., Lagor, W. R., Birkeland, A., Levin, M., Li, X., Robblee, M., Fedorov, V. D., Yamamoto, M., Satoh, T., Akira, S., Kathiresan, S., Breslow, J. L., & Rader, D. J. (2010). Trib1 is a lipid- and myocardial infarction-associated gene that regulates hepatic lipogenesis and vldl production in mice. *Journal of Clinical Investigation*, *120*, 4410–4414.[CrossRef].

Callis, T. E., Pandya, K., Seok, H. Y., Tang, R. H., Tatsuguchi, M., Huang, Z. P., Chen, J. F., Deng, Z., Gunn, B., Shumate, J., Willis, M. S., Selzman, C. H., & Wang, D. Z. (2009). Microrna-208a is a regulator of cardiac hypertrophy and conduction in mice. *Journal of Clinical Investigation*, *119*, 2772–2786.[CrossRef].

Cheng, M., Yang, J., Zhao, X., Zhang, E., Zeng, Q., Yu, Y., Yang, L., Wu, B., Yi, G., Mao, X., Huang, K., Dong, N., Xie, M., Limdi, N. A., Prabhu, S. D., Zhang, J., & Qin, G. (2019). Circulating myocardial microrna from infarcted hearts are carried in exosomes and mobilise bone marrow progenitor cells. *Nature Communication*, *10*, 019–08895.

Cleary, M. D., Meiering, C. D., Jan, E., Guymon, R., & Boothroyd, J. C. (2005). Biosynthetic labeling of rna with uracil phosphoribosyltransferase allows cell-specific microarray analysis of mrna synthesis and decay. *Nature Biotechnology*, *23*(2), 232–237. https://doi.org/10.1038/nbt1061[CrossRef]

Cui, Y., Zheng, Y., Liu, X., Yan, L., Fan, X., Yong, J., Hu, Y., Dong, J., Li, Q., Wu, X., Gao, S., Li, J., Wen, L., Qiao, J., & Tang, F. (2019). Single-cell transcriptome analysis maps the developmental track of the human heart. *Cell Reports*, *26*, 1934–1950.e5.[CrossRef].

de Abreu, R. C., Fernandes, H., da, C., Martins, P. A., Sahoo, S., Emanueli, C., & Ferreira, L. (2020). Native and bioengineered extracellular vesicles for cardiovascular therapeutics. *Nature Reviews Cardiology*, *17*, 685–697.[CrossRef].

Deatherage, B. L., & Cookson, B. T. (2012). Membrane vesicle release in bacteria, eukaryotes, and archaea: A conserved yet underappreciated aspect of microbial life. *Infection and Immunity*, *80*, 1948–1957.[CrossRef].

de Couto, G., Gallet, R., Cambier, L., Jaghatspanyan, E., Makkar, N., Dawkins, J. F., Berman, B. P., & Marbán, E. (2017). Exosomal microrna transfer into macrophages mediates cellular postconditioning. *Circulation*, *136*, 200–214.[CrossRef].

Efendigil, M. C., Harley, A., Deegan, T., & McKendrick, C. S. (1975). Changes in glomerular filtration rate following myocardial infarction. *Cardiovascular Research*, *9*, 741–744.[CrossRef].

Fu, L., Wang, H., Liao, Y., Zhou, P., Xu, Y., Zhao, Y., Xie, S., Zhao, S., & Li, X. (2020). Mir-208b modulating skeletal muscle development and energy homoeostasis through targeting distinct targets. *RNA Biology*, *17*, 743–754.[CrossRef].

Gao, E., Lei, Y. H., Shang, X., Huang, Z. M., Zuo, L., Boucher, M., Fan, Q., Chuprun, J. K., Ma, X. L., & Koch, W. J. (2010). A novel and efficient model of coronary artery ligation and myocardial infarction in the mouse. *Circulation Research*, *107*, 1445–1453.[CrossRef].

Gao, L., Wang, L., Wei, Y., Krishnamurthy, P., Walcott, G. P., Menasché, P., & Zhang, J. (2020). Exosomes secreted by hipsc-derived cardiac cells improve recovery from myocardial infarction in swine. *Science Translational Medicine*, *12*, eaay1318.

Garikipati, V. N. S., Shoja-Taheri, F., Davis, M. E., & Kishore, R. (2018). Extracellular vesicles and the application of system biology and computational modeling in cardiac repair. *Circulation Research*, *123*, 188–204.[CrossRef].

Gay, L., Karfilis, K. V., Miller, M. R., Doe, C. Q., & Stankunas, K. (2014). Applying thiouracil tagging to mouse transcriptome analysis. *Nature Protocols*, *9*, 410–420.[CrossRef].

Gay, L., Miller, M. R., Ventura, P. B., Devasthali, V., Vue, Z., Thompson, H. L., Temple, S., Zong, H., Cleary, M. D., Stankunas, K., & Doe, C. Q. (2013). Mouse tu tagging: A chemical/genetic intersectional method for purifying cell type-specific nascent rna. *Genes & Development*, *27*, 98–115.

Gholamin, S., Pasdar, A., Khorrami, M. S., Mirzaei, H., Mirzaei, H. R., Salehi, R., Ferns, G. A., Ghayour-Mobarhan, M., & Avan, A. (2016). The potential for circulating micrornas in the diagnosis of myocardial infarction: A novel approach to disease diagnosis and treatment. *Current Pharmaceutical Design*, *22*, 397–403.[CrossRef].

Grueter, C. E., van Rooij, E., Johnson, B. A., DeLeon, S. M., Sutherland, L. B., Qi, X., Gautron, L., Elmquist, J. K., Bassel-Duby, R., & Olson, E. N. (2012). A cardiac microrna governs systemic energy homeostasis by regulation of med13. *Cell*, *149*, 671–683.[CrossRef].

Guazzi, M., Arena, R., & Guazzi, M. D. (2008). Evolving changes in lung interstitial fluid content after acute myocardial infarction: Mechanisms and pathophysiological correlates. *American Journal of Physiology. Heart and Circulatory Physiology*, *294*, 11.[CrossRef].

Hales, C. A., & Kazemi, H. (1974). Small-airways function in myocardial infarction. *New England Journal of Medicine*, *290*, 761–765.[CrossRef].

Han, C., Yang, J., Sun, J., & Qin, G. (2022). Extracellular vesicles in cardiovascular disease: Biological functions and therapeutic implications. *Pharmacology & Therapeutics*, *233*, 108025.

Herzog, V. A., Reichholf, B., Neumann, T., Rescheneder, P., Bhat, P., Burkard, T. R., Wlotzka, W., von Haeseler, A., Zuber, J., & Ameres, S. L. (2017). Thiol-linked alkylation of rna to assess expression dynamics. *Nature Methods*, *14*, 1198–1204.[CrossRef].

Hirooka, Y. (2010). Brain perivascular macrophages and central sympathetic activation after myocardial infarction: Heart and brain interaction. *Hypertension*, *55*, 610–611.[CrossRef].

Horak, M., Novak, J., & Bienertova-Vasku, J. (2016). Muscle-specific micrornas in skeletal muscle development. *Developmental Biology*, *410*, 1–13.[CrossRef].

Hu, L. J., Ren, W. Y., Shen, Q. J., Ji, H. Y., & Zhu, L. (2017). Inflammation in lung after acute myocardial infarction is induced by dendritic cell-mediated immune response. *Journal of Biological Regulators and Homeostatic Agents*, *31*, 29–40.

Huang, F., Na, N., Ijichi, T., Wu, X., Miyamoto, K., Ciullo, A., Tran, M., Li, L., Ibrahim, A., Marbán, E., & de Couto, G. (2021). Exosomally derived y rna fragment alleviates hypertrophic cardiomyopathy in transgenic mice. *Molecular Therapy. Nucleic Acids*, *24*, 951–960.[CrossRef].

Huang, T., Alvarez, A. A., Pangeni, R. P., Horbinski, C. M., Lu, S., Kim, S. H., James, C. D., JR, J., AK, J., Brenann, C. W., Sulman, E. P., Finocchiaro, G., Tan, M., Nishikawa, R., Lu, X., Nakano, I., Hu, B., & Cheng, S. Y. (2016). A regulatory circuit of mir-125b/mir-20b and wnt signalling controls glioblastoma phenotypes through fzd6-modulated pathways. *Nature Communication*, *7*, 12885.[CrossRef].

Jasmin, J. F., Calderone, A., Leung, T. K., Villeneuve, L., & Dupuis, J. (2003). Lung structural remodeling and pulmonary hypertension after myocardial infarction: Complete reversal with irbesartan. *Cardiovascular Research*, *58*, 621–631.[CrossRef].

Jasmin, J. F., Mercier, I., Hnasko, R., Cheung, M. W., Tanowitz, H. B., Dupuis, J., & Lisanti, M. P. (2004). Lung remodeling and pulmonary hypertension after myocardial infarction: Pathogenic role of reduced caveolin expression. *Cardiovascular Research*, *63*, 747–755.[CrossRef].

Kang, M., Jordan, V., Blenkiron, C., & Chamley, L. W. (2021). Biodistribution of extracellular vesicles following administration into animals: A systematic review. *Journal of Extracellular Vesicles*, *10*, e12085.[CrossRef].

Ke, H., Masoumi, K. C., Ahlqvist, K., Seckl, M. J., Rydell-Törmänen, K., & Massoumi, R. (2016). Nemo-like kinase regulates the expression of vascular endothelial growth factor (vegf) in alveolar epithelial cells. *Science Reports*, *6*, 23987.[CrossRef].

Kishore, R., & Khan, M. (2017). Cardiac cell-derived exosomes: Changing face of regenerative biology. *European Heart Journal*, *38*(3), 212–215. https://doi.org/10.1093/eurheartj/ehw324[CrossRef]

Li, X., Bi, H., Xie, S., & Cui, W. (2022). Mir-208b regulates the conversion of skeletal muscle fiber types by inhibiting mettl8 expression. *Frontiers in Genetics*, *13*, 820464.[CrossRef].

Ling, L. H., Rogers, S. M., Tay, V., Limmon, G. V., Dahai, Z., & Rogers, K. (2009). Comparison of various tissue-preparation techniques for cryosectioning of frozen mouse tissues. *Journal of Histotechnology*, *32*, 186–189.[CrossRef].

Lisak, D., Schacht, T., Gawlitza, A., Albrecht, P., Aktas, O., Koop, B., Gliem, M., Hofstetter, H. H., Zanger, K., Bultynck, G., Parys, J. B., De Smedt, H., Kindler, T., Adams-Quack, P., Hahn, M., Waisman, A., Reed, J. C., Hövelmeyer, N., & Methner, A. (2016). Bax inhibitor-1 is a ca(2+) channel critically important for immune cell function and survival. *Cell Death and Differentiation*, *23*, 358–368.[CrossRef].

Liu, X., Yuan, L., Chen, F., Zhang, L., Chen, X., Yang, C., & Han, Z. (2017). Circulating mir-208b: A potentially sensitive and reliable biomarker for the diagnosis and prognosis of acute myocardial infarction. *Clinical Laboratory*, *63*, 101–109.[CrossRef].

Liu, Z., Diep, C., Mao, T., Huang, L., Merrill, R., Zhang, Z., & Peng, Y. (2015). Microrna-92b promotes tumor growth and activation of nf-kappab signaling via regulation of nlk in oral squamous cell carcinoma. *Oncology Reports*, *34*, 2961–2968.[CrossRef].

Lompre, A. M., Nadal-Ginard, B., & Mahdavi, V. (1984). Expression of the cardiac ventricular alpha- and beta-myosin heavy chain genes is developmentally and hormonally regulated. *Journal of Biological Chemistry*, *259*, 6437–6446.[CrossRef].

Loyer, X., Zlatanova, I., Devue, C., Yin, M., Howangyin, K. Y., Klaihmon, P., Guerin, C. L., Kheloufi, M., Vilar, J., Zannis, K., Fleischmann, B. K., Hwang, D. W., Park, J., Lee, H., Menasche, P., Silvestre, J. S., & Boulanger, C. M. (2018). Intra-cardiac release of extracellular vesicles shapes inflammation following myocardial infarction. *Circulation Research*, *123*, 100–106.[CrossRef].

Lunney, M., Ruospo, M., Natale, P., Quinn, R. R., Ronksley, P. E., Konstantinidis, I., Palmer, S. C., Tonelli, M., Strippoli, G. F., & Ravani, P. (2020). Pharmacological interventions for heart failure in people with chronic kidney disease. *Cochrane Database of Systematic Reviews (Online)*, *2*, CD012466.

Luo, W., Dai, Y., Chen, Z., Yue, X., Andrade-Powell, K. C., & Chang, J. (2020). Spatial and temporal tracking of cardiac exosomes in mouse using a nano-luciferase-cd63 fusion protein. *Communications Biology*, *3*, 020–0830.[CrossRef].

Mlczoch, J., & Kaindl, F. (1980). [abnormal pulmonary function in patients with acute uncomplicated myocardial infarction (author's transl)]. *Zeitschrift Fur Kardiologie*, *69*, 126–130.

Montgomery, R. L., Hullinger, T. G., Semus, H. M., Dickinson, B. A., Seto, A. G., Lynch, J. M., Stack, C., Latimer, P. A., Olson, E. N., & van Rooij, E. (2011). Therapeutic inhibition of mir-208a improves cardiac function and survival during heart failure. *Circulation*, *124*, 1537–1547.[CrossRef].

Nakano, H., Nakano, K., & Cook, D. N. (2018). Isolation and purification of epithelial and endothelial cells from mouse lung. *Type 2 Immunity. Methods in Molecular Biology*, *1799*, 59–69.[CrossRef].

O'Brien, K., Breyne, K., Ughetto, S., Laurent, L. C., & Breakefield, X. O. (2020). Rna delivery by extracellular vesicles in mammalian cells and its applications. *Nature Reviews Molecular Cell Biology*, *21*, 585–606.[CrossRef].

Oh, J. G., Lee, P., Gordon, R. E., Sahoo, S., Kho, C., & Jeong, D. (2020). Analysis of extracellular vesicle mirna profiles in heart failure. *Journal of Cellular and Molecular Medicine*, *24*, 7214–7227.[CrossRef].

Peinado, H., Alečković, M., Lavotshkin, S., Matei, I., Costa-Silva, B., Moreno-Bueno, G., Hergueta-Redondo, M., Williams, C., García-Santos, G., Ghajar, C., Nitadori-Hoshino, A., Hoffman, C., Badal, K., Garcia, B. A., Callahan, M. K., Yuan, J., Martins, V. R., Skog, J., Kaplan, R. N., …, Lyden, D. (2012). Melanoma exosomes educate bone marrow progenitor cells toward a pro-metastatic phenotype through met. *Nature Medicine*, *18*, 883–891.[CrossRef].

Prabhu, S. D., & Frangogiannis, N. G. (2016). The biological basis for cardiac repair after myocardial infarction: From inflammation to fibrosis. *Circulation Research*, *119*, 91–112.[CrossRef].

Rädle, B., Rutkowski, A. J., Ruzsics, Z., Friedel, C. C., Koszinowski, U. H., & Dölken, L. (2013). Metabolic labeling of newly transcribed rna for high resolution gene expression profiling of rna synthesis, processing and decay in cell culture. *Journal of visualized experiments: JoVE*, *8*, 50195.

Raposo, G., Nijman, H. W., Stoorvogel, W., Liejendekker, R., Harding, C. V., Melief, C. J., & Geuze, H. J. (1996). B lymphocytes secrete antigen-presenting vesicles. *Journal of Experimental Medicine*, *183*, 1161–1172.[CrossRef].

Raposo, G., & Stoorvogel, W. (2013). Extracellular vesicles: Exosomes, microvesicles, and friends. *Journal of Cell Biology*, *200*, 373–383.[CrossRef].

Rivoli, L., Vliegenthart, A. D., de Potter, C. M., van Bragt, J. J., Tzoumas, N., Gallacher, P., Farrah, T. E., Dhaun, N., & Dear, J. W. (2017). The effect of renal dysfunction and haemodialysis on circulating liver specific mir-122. *British Journal of Clinical Pharmacology*, *83*, 584–592.[CrossRef].

Robinson, D. G., Ding, Y., & Jiang, L. (2016). Unconventional protein secretion in plants: A critical assessment. *Protoplasma*, *253*, 31–43.[CrossRef].

Sahoo, S., & Losordo, D. W. (2014). Exosomes and cardiac repair after myocardial infarction. *Circulation Research*, *114*, 333–344.[CrossRef].

Sharma, U., Conine, C. C., Shea, J. M., Boskovic, A., Derr, A. G., Bing, X. Y., Belleannee, C., Kucukural, A., Serra, R. W., Sun, F., Song, L., Carone, B. R., Ricci, E. P., Li, X. Z., Fauquier, L., Moore, M. J., Sullivan, R., Mello, C. C., Garber, M., & Rando, O. J. (2016). Biogenesis and function of trna fragments during sperm maturation and fertilization in mammals. *Science*, *351*, 391–396.[CrossRef].

Sharma, U., Sun, F., Conine, C. C., Reichholf, B., Kukreja, S., Herzog, V. A., Ameres, S. L., & Rando, O. J. (2018). Small rnas are trafficked from the epididymis to developing mammalian sperm. *Developmental Cell*, *46*, 481–494.[CrossRef].

Song, J. J., Yang, M., Liu, Y., Song, J. W., Wang, J., Chi, H. J., Liu, X. Y., Zuo, K., Yang, X. C., & Zhong, J. C. (2020). Microrna-122 aggravates angiotensin ii-mediated apoptosis and autophagy imbalance in rat aortic adventitial fibroblasts via the modulation of sirt6-elabela-ace2 signaling. *European Journal of Pharmacology*, *883*, 173374.[CrossRef].

Tang, T. T., Li, Y. Y., Li, J. J., Wang, K., Han, Y., Dong, W. Y., Zhu, Z. F., Xia, N., Nie, S. F., Zhang, M., Zeng, Z. P., Lv, B. J., Jiao, J., Liu, H., Xian, Z. S., Yang, X. P., Hu, Y., Liao, Y. H., Wang, Q., …, Cheng, X. (2018). Liver-heart crosstalk controls il-22 activity in cardiac protection after myocardial infarction. *Theranostics*, *8*, 4552–4562.[CrossRef].

Tardiff, J. C., Hewett, T. E., Factor, S. M., Vikstrom, K. L., Robbins, J., & Leinwand, L. A. (2000). Expression of the beta (slow)-isoform of mhc in the adult mouse heart causes dominant-negative functional effects. *American Journal of Physiology. Heart and Circulatory Physiology*, *278*, H412–H419.[CrossRef].

Thackeray, J. T., Hupe, H. C., Wang, Y., Bankstahl, J. P., Berding, G., Ross, T. L., Bauersachs, J., Wollert, K. C., & Bengel, F. M. (2018). Myocardial inflammation predicts remodeling and neuroinflammation after myocardial infarction. *Journal of the American College of Cardiology*, *71*, 263–275.[CrossRef].

Tomorsky, J., DeBlander, L., Kentros, C. G., Doe, C. Q., & Niell, C. M. (2017). Tu-tagging: A method for identifying layer-enriched neuronal genes in developing mouse visual cortex. *eNeuro*, *4*, 0181–0117.[CrossRef].

Valadi, H., Ekström, K., Bossios, A., Sjöstrand, M., Lee, J. J., & Lötvall, J. O. (2007). Exosome-mediated transfer of mrnas and micrornas is a novel mechanism of genetic exchange between cells. *Nature Cell Biology*, *9*, 654–659.[CrossRef].

van Niel, G., D'Angelo, G., & Raposo, G. (2018). Shedding light on the cell biology of extracellular vesicles. *Nature Reviews Molecular Cell Biology*, *19*, 213–228.[CrossRef].

van Rooij, E., Quiat, D., Johnson, B. A., Sutherland, L. B., Qi, X., Richardson, J. A., Kelm, R. J. Jr., & Olson, E. N. (2009). A family of micrornas encoded by myosin genes governs myosin expression and muscle performance. *Developmental Cell*, *17*, 662–673.[CrossRef].

van Rooij, E., Sutherland, L. B., Qi, X., Richardson, J. A., Hill, J., & Olson, E. N. (2007). Control of stress-dependent cardiac growth and gene expression by a microrna. *Science*, *316*, 575–579.[CrossRef].

Verweij, F. J., Balaj, L., Boulanger, C. M., Carter, D. R. F., Compeer, E. B., D'Angelo, G., El Andaloussi, S., Goetz, J. G., Gross, J. C., Hyenne, V., Kramer-Albers, E. M., Lai, C. P., Loyer, X., Marki, A., Momma, S., Nolte-'t Hoen, E. N. M., Pegtel, D. M., Peinado, H., Raposo, G., …, van Niel, G. (2021). The power of imaging to understand extracellular vesicle biology in vivo. *Nature Methods*, *18*, 1013–1026.[CrossRef].

Virani, S. S., Alonso, A., Benjamin, E. J., Bittencourt, M. S., Callaway, C. W., Carson, A. P., Chamberlain, A. M., Chang, A. R., Cheng, S., Delling, F. N., Djousse, L., Elkind, M. S. V., Ferguson, J. F., Fornage, M., Khan, S. S., Kissela, B. M., Knutson, K. L., Kwan, T. W., Lackland, D. T., …, Tsao, C. W. (2020). Heart disease and stroke statistics-2020 update: A report from the american heart association. *Circulation*, *141*, e139–e596.[CrossRef].

Wang, J., Song, C., Cao, X., Li, H., Cai, H., Ma, Y., Huang, Y., Lan, X., Lei, C., Ma, Y., Bai, Y., Lin, F., & Chen, H. (2019). Mir-208b regulates cell cycle and promotes skeletal muscle cell proliferation by targeting cdkn1a. *Journal of Cellular Physiology*, *234*, 3720–3729.[CrossRef].

Werner, R. A., Hess, A., Koenig, T., Diekmann, J., Derlin, T., Melk, A., Thackeray, J. T., Bauersachs, J., & Bengel, F. M. (2021). Molecular imaging of inflammation crosstalk along the cardio-renal axis following acute myocardial infarction. *Theranostics*, *11*, 7984–7994.[CrossRef].

Wilkes, M. C., Jung, K., Lee, B. E., Saxena, M., Sathianathen, R. S., Mercado, J. D., Perez, C., Flygare, J., Narla, A., Glader, B., & Sakamoto, K. M. (2021). The active component of ginseng, ginsenoside rb1, improves erythropoiesis in models of diamond-blackfan anemia by targeting nemo-like kinase. *Journal of Biological Chemistry*, *297*, 100988.[CrossRef].

Xu, R., Zhang, Z. Z., Chen, L. J., Yu, H. M., Guo, S. J., Xu, Y. L., Oudit, G. Y., Zhang, Y., Chang, Q., Song, B., Chen, D. R., Zhu, D. L., & Zhong, J. C. (2016). Ascending aortic adventitial remodeling and fibrosis are ameliorated with apelin-13 in rats after tac via suppression of the mirna-122 and lgr4-beta-catenin signaling. *Peptides*, *86*, 85–94.[CrossRef].

Yan, X., Liu, J., Wu, H., Liu, Y., Zheng, S., Zhang, C., & Yang, C. (2016). Impact of mir-208 and its target gene nemo-like kinase on the protective effect of ginsenoside rb1 in hypoxia/ischemia injuried cardiomyocytes. *Cellular Physiology and Biochemistry*, *39*, 1187–1195.[CrossRef].

Yanez-Mo, M., Siljander, P. R., Andreu, Z., Zavec, A. B., Borras, F. E., Buzas, E. I., Buzas, K., Casal, E., Cappello, F., Carvalho, J., Colas, E., Cordeiro-da Silva, A., Fais, S., Falcon-Perez, J. M., Ghobrial, I. M., Giebel, B., Gimona, M., Graner, M., Gursel, I., …, De Wever, O. (2015). Biological properties of extracellular vesicles and their physiological functions. *Journal of Extracellular Vesicles*, *4*, 27066.[CrossRef].

Yang, J., Yu, X., Xue, F., Li, Y., Liu, W., & Zhang, S. (2018). Exosomes derived from cardiomyocytes promote cardiac fibrosis via myocyte-fibroblast cross-talk. *American Journal of Translational Research*, *10*, 4350–4366.

Yasuda, J., Yokoo, H., Yamada, T., Kitabayashi, I., Sekiya, T., & Ichikawa, H. (2004). Nemo-like kinase suppresses a wide range of transcription factors, including nuclear factor-kappab. *Cancer Science*, *95*, 52–57.[CrossRef].

Youn, S. W., Li, Y., Kim, Y. M., Sudhahar, V., Abdelsaid, K., Kim, H. W., Liu, Y., Fulton, D. J. R., Ashraf, M., Tang, Y., Fukai, T., & Ushio-Fukai, M. (2019). Modification of cardiac progenitor cell-derived exosomes by mir-322 provides protection against myocardial infarction through nox2-dependent angiogenesis. *Antioxidants*, *8*, 18.

Zaborowski, M. P., Balaj, L., Breakefield, X. O., & Lai, C. P. (2015). Extracellular vesicles: Composition, biological relevance, and methods of study. *Bioscience*, *65*, 783–797.[CrossRef].

Zeiner, G. M., Cleary, M. D., Fouts, A. E., Meiring, C. D., Mocarski, E. S., & Boothroyd, J. C. (2008). Rna analysis by biosynthetic tagging using 4-thiouracil and uracil phosphoribosyltransferase. *Methods in Molecular Biology*, *419*, 135–146.[CrossRef].

Zhang, S., Zhang, R., Wu, F., & Li, X. (2018). Microrna-208a regulates h9c2 cells simulated ischemia-reperfusion myocardial injury via targeting chd9 through notch/nf-kappa b signal pathways. *International Heart Journal*, *59*, 580–588.[CrossRef].

Zilahi, E., Adamecz, Z., Bodoki, L., Griger, Z., Poliska, S., Nagy-Vincze, M., & Danko, K. (2019). Dysregulated expression profile of myomirs in the skeletal muscle of patients with polymyositis. *Ejifcc [Electronic Resource]*, *30*, 237–245.

SUPPORTING INFORMATION

Additional supporting information can be found online in the Supporting Information section at the end of this article.

How to cite this article: Han, C., Yang, J., Zhang, E., Jiang, Y., Qiao, A., Du, Y., Zhang, Q., An, J., Sun, J., Wang, M., Nguyen, T., Lal, H., Krishnamurthy, P., Zhang, J., & Qin, G. (2022). Metabolic labeling of cardiomyocyte-derived small extracellular-vesicle (sEV) miRNAs identifies miR-208a in cardiac regulation of lung gene expression. *Journal of Extracellular Vesicles*, *11,* e12246. https://doi.org/10.1002/jev2.12246